[23]C. Domb and M. F. Sykes, J. Math. Phys. 2, 63 (1961).
[24]G. A. Baker, Jr., Advan. Theoret. Phys. 1, 1 (1965).
[25]Close-packed lattices contain polygons with an odd and even number of lines, while for loose-packed lattices only polygons with an even number of lines occur.
[26]The result for the simple quadratic lattice was briefly reported by J. F. Nagle (Ref. 18, Sec. VB).
[27]M. F. Sykes, J. W. Essam, and D. S. Gaunt, J. Math. Phys. 6, 283 (1965).
[28]D. S. Gaunt and M. E. Fisher, J. Chem. Phys. 43, 2840 (1965); D. S. Gaunt, *ibid.* 46, 3237 (1967).
[29]The $[M, N]$ Padé approximant to the Dlog w series of $f(w)$ is the ratio of a polynomial $P(w)$ of degree M to a polynomial $Q(w)$ of degree N, their coefficients being chosen so that the expansion of $P(w)/Q(w)$ agrees with the expansion of $(d/dw)\ln f(w)$ up to degree $(M+N)$. We have restricted attention to the cases when $M=N+1$, N, $N-1$.

PHYSICAL REVIEW VOLUME 179, NUMBER 1 5 MARCH 1969

Measurements of Lateral Diffusion Coefficients and First Townsend Coefficients for Electrons in Helium by an Electron-Density Sampling Method*

G. Cavalleri
Centro Informazioni Studi Esperienze, C. P. 3986, 20100 *Milano, Italy*
(Received 11 September 1968)

Direct experimental measurements of electron diffusion coefficients D in helium have been carried out at 300°K in the range of $0 \leq E/N < 2.7\times10^{-16}$ V cm^2 ($0 \leq E/P_0 < 10$ V cm^{-1} Torr^{-1}) by an improved electron-density sampling method. Absolute errors less than ± 0.5% are claimed in the range $0 \leq E/N < 9\times10^{-17}$ V cm^2 and less than 1.5% in the range $9\times10^{-17} < E/N < 2.7\times10^{-16}$ V cm^2.

The obtained values of D are in agreement with those of Crompton, Elford, and Jory in the range of $2.124\times10^{-19} \leq E/N \leq 3.03\times10^{-17}$ V cm^2 studied by these authors. Also measurements of αW (where α is Townsend's first coefficient and W the drift velocity) have been performed in the range $9.03\times10^{-17} \leq E/N \leq 2.6\times10^{-16}$ V cm^2 (corresponding to $3.2 \leq E/P_0 \leq 10$ V cm^{-1} Torr^{-1}). Values of α with an accuracy evaluated at ± 10% are obtained by dividing αW by the W values found in the literature. These α values are to be compared with those of the literature, which are dispersed by a factor of 3 in the above range.

(1) INTRODUCTION

The normal procedure[1] to obtain free diffusion coefficients D consists in the measurements of the drift velocity W (and hence of the mobility $\mu = W/E$, where E is the electric field strength) and of the ratio D/μ, from which $D = \mu(D/\mu)$. Consequently, values at $E/N = 0$ (where N is the molecule number density) are not achievable. Direct measurements of D at $E/N = 0$ are in principle possible by the microwave method[2] but, because of the high ionic concentration during the microwave breakdown and the small values of ion diffusion coefficients with respect to electron diffusion coefficients, what is actually measured is an ambipolar diffusion coefficient. Namely, even when only one free electron (detectable by Carruther's[3] method – though with an accuracy of ± 40%) remains an average in the measuring chamber, the number of ions inside the measuring chamber is so high that the electric field due to ion spatial charge considerably affects electron diffusion.

On the contrary direct measurements of electron free diffusion coefficients D at $E/N = 0$ with an accuracy of ± 0.5% have been performed by the method used here, which is an improvement of the sampling method, already described by Cavalleri, Gatti, and Principi.[4] This method would also allow measurements of metastable mean lives, electron attachment coefficients, and thermalization times. By an auxiliary sinusoidal, "heating" electric field, D has been measured as a function of E/N from zero values up to $E/N = 2.65\times10^{-16}$ V cm^2 (corresponding to $E/p_0 = 9.41$ V cm^{-1} Torr^{-1}, where p_0 is gas pressure reduced to 273°K). Also

measurements of αW (where α is Townsend's first coefficient) have been carried out by the new method, starting from E/p_0 values where Townsend's "avalanche" multiplication appreciably compensates electron losses due to diffusion to the chamber walls.

Dividing αW by the corresponding values of drift velocity W found in the literature, values of α in the range $9.03\times10^{-17} \leq E/N \leq 2.65\times10^{-16}$ V cm^2 ($3.2 \leq E/p \leq 9.41$ V cm^{-1} Torr^{-1}) are obtained. In this range the most recent α values found in the literature are dispersed by a factor of 6 if including theoretical values and by a factor of 3 if considering experimental values only [see Sec. 4 (4.3) and Ref. 29].

(2) EXPERIMENTAL APPARATUS

(2.1) Working Principles

A short x-ray pulse produces a primary ionization inside a cylindrical chamber containing the gas under examination. After a known delay t_1 from the end of the x-ray pulse, a strong voltage sampling pulse is applied to the chamber bases, consisting of two metal electrodes. The voltage pulse (which is a damped radio-frequency oscillation) produces as many Townsend's avalanches as the free electrons still present in the measuring chamber. The light emitted by the excited atoms in Townsend's avalanches is converted into a proportional electric pulse of amplitude A by a photomultiplier tube. Therefore the mean amplitude $\bar{A}$ is proportional to the mean number $\bar{n}$ of the electrons which are present in the measuring chamber after the time interval t_1. After the sampling pulse, a clearing voltage is applied to the electrodes in order to drag the ions out of the measuring chamber. Then a second cycle can be started. Actually, to avoid the effects due to instrumental drifts, a different known delay t_2 (between the end of the x-ray pulse and the voltage-sampling pulse) is introduced into the second cycle. In the third cycle there is again the first delay t_1, i.e., two different delays are alternated. Hence the ratio of the mean values, or better, of the centroids, of the two resulting amplitude-pulse spectra at the output of the photomultiplier, gives the ratio of the mean values of the surviving electrons after the delays t_1 and t_2, respectively. The clearing voltage can be either of the same sign (positive or negative) or alternate. In order to have symmetry with respect to the two different delays, two successive clearing pulses are positive and the successive pulse couple is negative, so that a complete cycle appears as sketched in Fig. 1. This cycle turned out to be the best one, since impurity ions (due both to ionization and electron attachment), accumulated on (or adsorbed asymmetrically by) only one electrode, originate contact potentials by Volta effects. If the clearing voltage is not symmetrical, these Volta potentials slowly increase and therefore it is not possible to balance them rigorously, as done for constant Volta effects [which can be compensated by external polarizations: See Sec. 2 (2.2)].

The duty cycle of Fig. 1 is used to measure the decrease of the mean electron number $\bar{n}$ versus time t in the absence of the electric field E. In order to have $\bar{n} = \bar{n}(t)$ in the case of a given E/N value, a sinusoidal voltage of constant amplitude is applied between the chamber electrodes.

Voltage frequency and gas pressure are selected so that the oscillating electric field is equivalent, with respect to diffusion, to a constant (dc) "heating" field [see Sec. 3 (3.2)].

From the experimental knowledge of the decay of the electron number $\bar{n} = \bar{n}(t)$ at different pressures, it is possible to deduce the electron diffusion coefficients D, the quantity $\sigma_{att} N\bar{c}$ (where $\bar{c}$ is the electron thermal velocity and σ_{att} the attachment cross section), the quantity αW and the decay time constants τ_m of metastable atoms. Namely, let us consider a gaseous binary mixture, whose most abundant gas ("principal gas") has a molecule concentration N and the other (considered as an impurity) has a concentration $N^* \ll N$. The impurity gas undergoes Penning's effect, i.e., can be ionized on collision with the principal gas metastable molecules. In the diffusion approximation the equation governing the electron concentration N_e is given by

$$\frac{\partial N_e}{\partial t} = D\nabla^2 N_e + \alpha W N_e - \sigma_{att} N\bar{c} N_e - \sigma_{att}{}^* N^* \bar{c} N_e + K N^* . \quad (1)$$

The quantity K, which appears in the term KN^* accounting for Penning's effect, is given by

$$K = \sum \beta_s N_{ms} , \quad (2)$$

where N_{ms} is the concentration of the sth type of metastable molecules and β_s the de-excitation rate for $N^* = N_{ms} = 1$ by Penning's effect (due to collisions between the principal gas metastable molecules and impurity molecules).

In the case of $N^* = 0$, absence of attachment (as occurs for noble gases) and $\alpha = 0$ (low E/N), Eq. (1) reduces to the pure diffusion equation, whose solution for a cylindrical measuring chamber is given by[5]

$$N_e(r,z,t) = \sum_{i,j=1}^{\infty} f_{ij}(r,z)\, e^{-t/\tau_{ij}} , \quad (3)$$

where $f_{ij}(xyz)$ is a set of orthonormal eigenfunctions of the diffusion equation. After a time of the order of one time constant of the fundamental

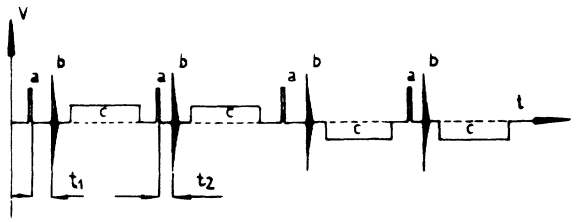

FIG. 1. Complete duty cycle: a represents x-ray pulse; b sampling amplification pulse; c clearing field, t_1 and t_2 the two different alternate delays between the ends of x-ray bursts and sampling pulses.

mode (the second mode has an associated time constant about 9 times smaller), i.e., for $t < \tau_{11}$, the mean spatial distribution or the total number n of electrons contained in the chamber [obtained by integrating Eq. (3) over the spatial coordinates] is given by

$$n = n_{01} e^{-t/\tau_{11}}, \tag{4}$$

where τ_{11} is related to the radius R and the height H of the chamber [see Sec. 2 (2.2) and Fig. 3] by the expression[5]

$$\frac{1}{\tau_{11}} = \frac{D}{\Lambda_{11}^2} = D\left[\left(\frac{\pi}{H-2s}\right)^2 + \left(\frac{2.405}{R}\right)^2\right]. \tag{5}$$

Notice we have introduced no correction due to the extrapolation distance[6] 0.71λ (where λ is the electron mean free path) since it is negligible with respect to R and H in our working conditions. On the other hand, $H-2s$ is the effective height for diffusion since the electrons within a layer of width s at both electrodes are immediately captured, if s represents the mean drift length during a semiwave of the cw radio-frequency field:

$$s = 2W_M/\omega, \tag{6}$$

where W_M is the drift velocity relevant to the maximum value reached by the sinusoidal electric field in a period $2\pi/\omega$. This hypothesis (capture by any electrode of the electrons contained in an adjacent layer of thickness s) has been confirmed experimentally by using chambers of different heights and is supported by the work of Gill and von Engel.[7]

Hence, obtaining the time constant τ_{11} from experimental $\bar{n} = \bar{n}(t)$, it is possible to deduce the diffusion coefficient D by means of Eq. (5), and hence the reduced diffusion coefficients

$$D_{1N} = DN, \quad \text{or } D_{1p} = Dp_0. \tag{7}$$

In the more general case of Eq. (1), neglecting the modes higher than the fundamental one, we have

$$\frac{\partial N_e}{\partial t} = -N_e(D_{1N}/N\Lambda_{11}^2 - \alpha_{1N}NW + \sigma_{att}N\bar{c} + \sigma_{att}{}^*N^*\bar{c}) + N^*\sum\beta_s N_{ms}. \tag{8}$$

The quantity

$$\alpha_{1N} = \alpha/N, \quad (\text{or } \alpha_{1p} = \alpha/p_0) \tag{9}$$

is the reduced first Townsend coefficient which, like D_1 of Eq. (7), does not depend on the molecule concentration N. The metastable concentrations N_{ms} [which appear in Eqs. (2) and (8)] decay according to the law

$$N_{ms} = N_{ms0}e^{-t/\tau_{ms}} = N_{ms0}\exp[-t \times (D_{1ms}/N\Lambda_{11}^2 + \gamma_s N + \delta_s N^2 + \beta_s N^*)], \tag{10}$$

D_{1ms} being the diffusion coefficient reduced to $N=1$ of the sth metastable, γ_s and δ_s the de-excitation rate for $N=1$ by two-body and three-body collisions, respectively, and β_s the de-excitation rate for $N^* = N = 1$ by Penning's effect for the sth metastable. Higher modes for metastable diffusion have been neglected since the effect due to metastables is only a perturbation of the electron decay (up to delays of four electron-diffusion time constants).

Taking into account Eq. (10), the solution of Eq. (8), integrated over spatial variables gives

$$\bar{n} = Ae^{-t/\tau} + \sum_s B_s e^{-t/\tau_{ms}}, \tag{11}$$

where τ_{ms} is given by Eq. (10) and τ by

$$1/\tau = D_{1N}/N\Lambda_{11}^2 - \alpha_{1N}NW + \sigma_{att}N\bar{c} + \sigma_{att}{}^*N^*\bar{c}. \tag{12}$$

Therefore from the knowledge of the experimental curve $\bar{n} = \bar{n}(t)$ at different number densities N and N^*, the quantities contained in Eqs. (10) and (12) can be deduced.

In the present measurements pure helium has been used with standard high-vacuum techniques. The impurity concentration N^* has been estimated to be of the order of 10^{-6} with respect to helium concentration, and hence electron attachment is negligible (see Appendix A). Consequently Eq. (12) reduces to

$$1/\tau = D_{1N}/N\Lambda_{11}^2 - \alpha_{1N}NW. \tag{13}$$

Figure 2 shows typical experimental measure-

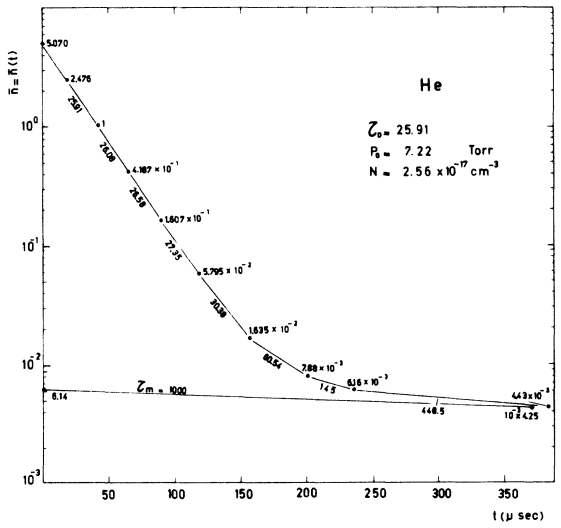

FIG. 2. Mean number $\bar{n}$ of the electrons remaining in the measuring chamber after the time t from the end of a x-ray pulse. Experimental points are obtained as ratios between the centroids of the light-amplitude spectra relevant to two different delays t_1 and t_2. Apparent time constants are indicated between corresponding couples of successive delays t_1 and t_2.

ments [here considered only in order to illustrate the method, the results of the set of performed measurements being fully discussed in Secs. 4 (4.2) and (4.3)] of the ratios $\bar{n}_1/\bar{n}_2$ between mean surviving electron numbers relevant to successive delay couples at $E/N=0$. The curve, partially plotted in Fig. 2 [the ordinates of which are proportional to $\bar{n}=\bar{n}(t)$] turned out to be well-fitted by Eq. (11) with three time constants, since in helium there are two types of metastables. The impurity concentration N^* being unknown, metastable time constants are of no importance, since the knowledge of the entire curve is significant only to accurately deduce the time constant τ appearing in Eqs. (11), (12), or (13). The calculated effects due to the two other terms turned out to be negligible in the delay range $25 < t < 50$ μsec. By two curves similar to the one of Fig. 2 performed at $E/N > 9.10^{-17}$ V cm^2 at different concentrations N, it is possible to obtain the two terms at the right side of Eq. (13) [see Secs. 3 (3.2) and 4 (4.3)].

Notice that the curve of Fig. 2 has been used starting from time delays larger than 25 μsec (corresponding to one diffusion time constant), since in the time interval $0 < t < 25$ μsec the effects due to higher modes are not negligible. Moreover the high-energy free electrons (up to 25 keV) produced by the x-ray pulse are still reaching thermal equilibrium during this time interval (for relaxation times see Appendix B).

(2.2) The Measuring Chamber

A sketch of the measuring chamber is shown in Fig. 3. It consists of a cylindrical envelope, made by Pyrex glass, containing two plane metal electrodes A and B, whose circular edges are very close to the glass wall so as to define a cylindrical volume of height H and diameter $2R$. The soft x rays enter this volume through a very small tube D capped by a small ball having a very thin wall (acting as an x-ray window). The glass lateral wall is metalized just outside the central strip of height H by a SnO_2 layer in order to have a low

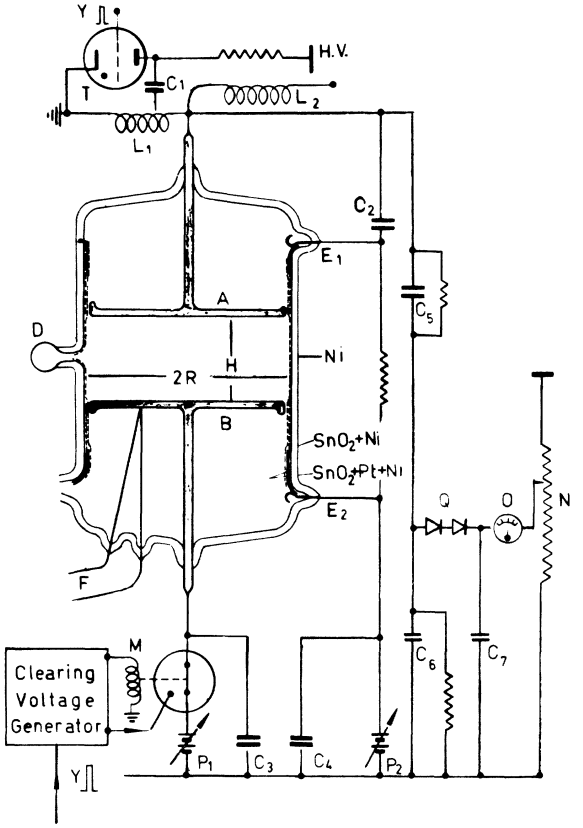

FIG. 3. Sketch of the measuring chamber and the main electrical connections. The electrodes A and B define a useful cylindrical volume of height H and diameter $2R$. The thin wall D acts as an x-ray window. E_1 and E_2 are electrical connections for the lateral semitransparent resistive layer. F is a thermocouple. P_1 and P_2 are variable polarizations to balance the work function difference. M is the relay coil, operated by the clearing voltage generator which is triggered at the end of the sampling pulse by pulse Y (see Fig. 5). Capacitors C_5 and C_6 (and relevant resistors) make up a calibrated voltage divider and Q_1, C_7, O, N a "peak sensing" potentiometric voltmeter to measure the cw radio-frequency field.

electrical resistance. Smaller strips of platinum partially covers the SnO_2 layer in correspondence with the contacts E_1 and E_2. These contacts are small springs sealed to small platinum plates resting on the platinum strips in order to have a low-resistance external connections. Finally nickel has been evaporated under vacuum on all lateral walls and the stainless-steel electrodes. The uniform resistive nickel layer satisfies the boundary condition of having a uniform field inside the useful volume when voltage differences are applied between the electrodes A and B. The damped oscillating pulse is applied by inductance L_1, acting as an autotransformer and as a part of an oscillating circuit together with the condenser C_1, to which a unidirectional pulse is applied by thyratron T, triggered after the desired delays from the end of the x-ray burst by pulse Y (see Fig. 5). A condenser C_2 acts as a short circuit between A and E_1 with respect to high frequency and as an open circuit with respect to constant (dc) voltages. A variable external resistance connects the contacts E_1 and E_2 to give the desired decay time constant to the damped radio-frequency pulse.

Gas temperature is measured by a thermocouple F and a potentiometer.

Despite the fact that all the useful volume walls are covered with the same material, residual work function differences (Volta effects) are still present but can be balanced by the external variable polarizations P_1 and P_2. The required voltages P_1 and P_2 are experimentally found as follows. Maintaining P_1 constants (for example zero), P_2 is varied and the corresponding values of the diffusion time constant τ or, more simply, of the ratios $\bar{n}_1/\bar{n}_2$ of the mean value of surviving electrons are measured. The delays t_1 and t_2 are chosen in the best range, i.e., between one and three time constants of the fundamental mode. For example, in the case of Fig. 2, convenient values are $t_1 = 25$ μsec and $t_2 = 50$ μsec. A typical curve of $\bar{n}_1/\bar{n}_2$ versus P_2 (mV) is shown in Fig. 4. Then the lateral polarization P_2 (between the electrodes A, B, and the lateral conducting layer) is fixed at the value P_{2M} corresponding to the minimum of $\bar{n}_1/\bar{n}_2$ (and therefore to the maximum of τ) and P_1 is varied so that a similar curve $\bar{n}_1/\bar{n}_2$ versus P_1 is obtained. Then P_1 is fixed in correspondence with the minimum value of $\bar{n}_1/\bar{n}_2$ and P_2 is again varied and a little change is found in the value of P_{2M}. Generally no further correction is found for a new search of P_{1M} (P_2 being fixed at the new value P_{2M}). The values of P_{1M} and P_{2M} so found are those required in order to balance work-function differences, since the diffusion time constant τ is maximum. Eventual work-function differences can still be present between different points of a same electrode or of the lateral conducting layer. It is possible, however, to consider their effects

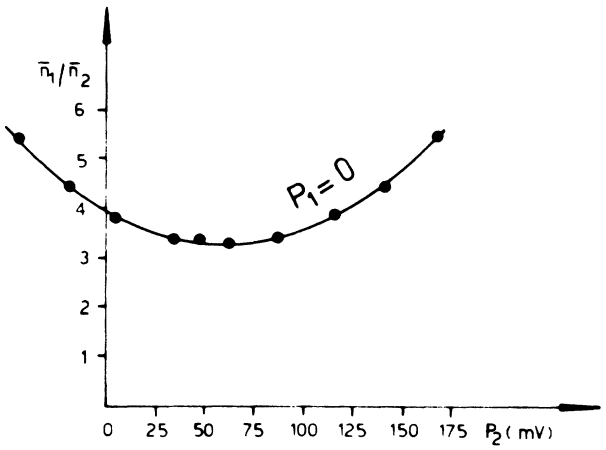

FIG. 4. Ratio $\bar{n}_1/\bar{n}_2$ of the mean numbers $\bar{n}_1$ and $\bar{n}_2$ of surviving electrons after the delays t_1 and t_2, respectively, versus polarization P_2 at constant polarization P_1 (see Fig. 3). The minimum of $\bar{n}_1/\bar{n}_2$ (corresponding to the maximum of the diffusion time constant τ) occurs for $P_2 \simeq 60$ mV.

as negligible, since the glass tube and stainless-steel electrodes have been accurately cleaned before the nickel evaporation, and the nickel layers have been obtained by eight symmetrical vacuum evaporations so as to have the best statistical uniformity for the layer. An indication in favor of the above hypothesis (that the effects due to eventual inhomogeneous work-function differences are negligible) comes from the fact that the polarization P_1, balancing contact potentials between the electrodes, turned out to be of the order of 10 mV (the two electrodes are made and covered by the same material). On the other hand, the polarization P_2, balancing Volta potentials between electrodes and lateral layer turned out to be up to 0.1 V. For example, in the case of Fig. 4 (relevant to a chamber with $H = 2.952$ cm and $R = 3.735$ cm) one has $P_2 \simeq 60$ mV. This result indicates that the nickel layer (which covers both electrodes and lateral glass wall) is so thin that it is affected by the type of material on which it is deposited.

For measurements with $E/N \neq 0$ a cw radio-frequency field is applied to the electrode A through a decoupling coil L_2. The amplitude of the continuous sinusoidal voltage is measured by means of a calibrated voltage divider (condenser C_5 and C_6 and relevant compensating resistors), a peak rectifier (Q and C_7), a precision potentiometer N, and a galvanometer O used as a null instrument. The constant stabilized voltage at the upper end of the potentiometer N is measured by a voltmeter with 0.1–0.2% accuracy. Condensers C_3 and C_4 act as short circuits with respect to the cw radio-frequency field and to the sampling pulse. Since

the accurate knowledge of the cw radio-frequency voltage between electrodes A and B is required, wire inductances and chamber capacitance have been calculated and measured in order to take into account the small voltage drops between electrode A and the application point of rectifier Q. It turns out that the voltage between electrodes A and B is 1% higher (resonance effect) than the voltage measured by the "peak-sensing potentiometric voltmeter" Q, C_7, O, and N. Actually two "peak voltmeters" have been used, one of them without voltage divider C_5 and C_6, i.e., directly connected with the external terminal of electrode A. This second peak voltmeter, which allows higher accuracy, can be used only if not applying sampling pulses, which might damage silicon diodes Q. The first peak voltmeter was used only to check possible small voltage changes when the second peak voltmeter was inserted. Finally silicon diode characteristics (current versus voltage) have been taken into account. By this method a ±0.5% overall accuracy in the measurement of the electric field strength E is claimed.

(2.3) The Electronic Equipment

The block scheme of the electronic layout is shown in Fig. 5. A network synchronizer and divider determines the duty cycle frequency. It delivers pulses at the maximum frequency of 50 Hz (standard frequency of European network) and its submultiples and triggers a univibrator (monostable multivibrator) giving the grid of a triode x-ray tube (normally cutoff) a rectangular pulse of 450-V amplitude and duration from 1 to 20 μsec. This pulse is properly phased with respect to the power network, in order to exploit the maximum thermionic emission (instant of the cathode maximum temperature) and to have a more stable intensity for the x-ray burst. A successive differentiator triggers, with the negative pulse (in correspondence with the trailing edge of the x-ray pulse), a bistable multivibrator (flip-flop) which, for successive pulses, alternatively switches univibrators I and II introducing two time delays t_1 and t_2. The ends of the delay pulses trigger (through two differentiators and an "or-circuit") the thyraton pulse generator applying the sampling pulse to electrode A of the measuring chamber and also furnishing a rectangular pulse Y in coincidence with the sampling pulse. Pulse Y triggers the clearing voltage generator which applies, after a "mechanical" delay due to relay commutation,

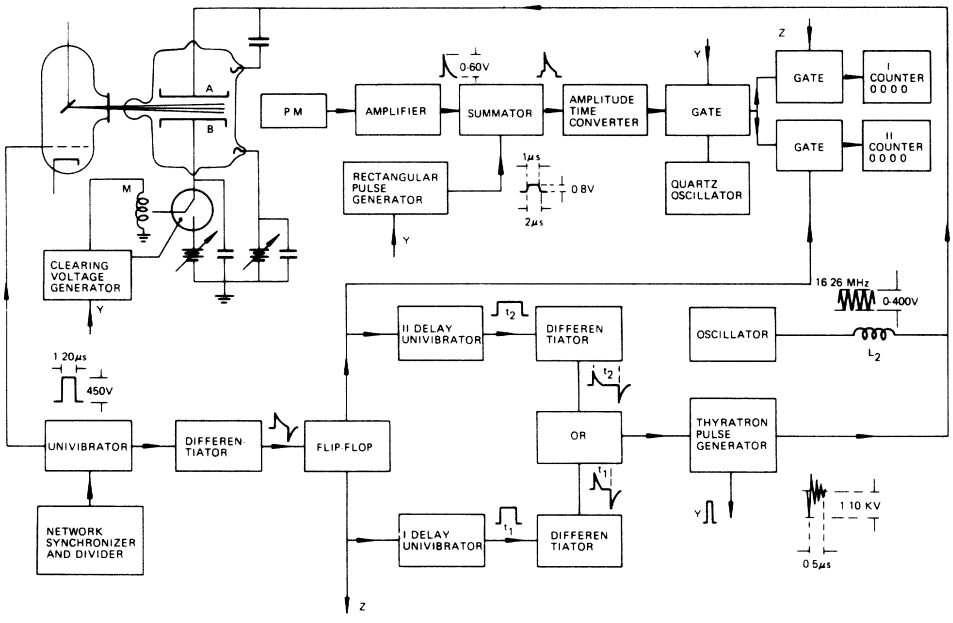

FIG. 5. Block scheme of the experimental apparatus. The "driving chain" begins with a synchronizer (with power network), "opens" an x-ray tube normally cutoff, applies the sampling pulse to the chamber electrodes after the delay t_1 (or t_2) introduced by univibrator I (or II) which is alternatively switched by a flip-flop, and finally applies the clearing voltage pulse to the chamber electrodes, with the sequence shown in Fig. 1. For measurements at $E/N \neq 0$ an oscillator gives the chamber electrodes a cw radio-frequency voltage of 16.26 MHz and amplitude variable from 0 to 400 V. The "measuring chain" begins with a photo-multiplier (P. M.) and ends with two pulse counters. The ratio of counter indications is equal to the ratio $\bar{n}_1/\bar{n}_2$ of the mean values (spectra centroids) $\bar{n}_1$ and $\bar{n}_2$ of the electrons remaining in the chamber after delays t_1 and t_2, respectively.

the clearing voltage to electrode B. A two flip-flop scaler, contained in the "clearing voltage generator," switches, after two successive pulses, the connection between two terminals of a voltage supply (furnishing a constant voltage variable from zero to ±200 V) in order to have the wave form (for the clearing voltage) shown in Fig. 1. The two delays t_1 and t_2 are accurately measured by a quartz oscillator clock, a gate and a counter.

The above description pertains to the "driving chain" used to measure $\bar{n} = \bar{n}(t)$ (see Fig. 2) in the case of $E/N = 0$. To perform measurements at $E/N \neq 0$, an oscillator applies a continuous sinusoidal voltage of 16.26 MHz to electrode A. The amplitude of the cw radio-frequency field can be changed between 0 and 400 V and is accurately measured between the terminals of electrodes A and B by means of the precision potentiometric method described at the end of the preceding Sec. 2 (2.2) (see also Fig. 3).

Let us now consider the "measuring chain." A photo-multiplier (P. M.) delivers to an amplifier an electric pulse A of amplitude proportional to the total light (emitted in consequence of the sampling amplification pulse), which is proportional to the number $\bar{n}$ of electrons remaining in the chamber at the sampling instant. In the case of small $\bar{n}$ values (high delays t_1 and t_2), it is convenient to add to pulse A a pedestal B of duration ($\simeq 2\mu$sec) approximately equal to the one of pulse A. Then two measurements of the same duration (for example, 10 minutes) are successively performed with and without measuring pulse A. The noise acts statistically in the same way on both measurements and therefore their subtraction reduces noise effects. Pulse A (with the eventual addition of pulse B), drives an "amplitude-to-time converter," which produces a pulse C whose duration is proportional to the amplitude of pulse A. Pulse C opens a gate circuit, through which passes a number of oscillations (generated by a quartz oscillator) proportional to amplitude A_s of sth pulse A. The gate circuit behaves also as a coincidence circuit since it operates only in coincidence with pulse Y, so eliminating most of the spurious pulses occurring casually (due to thermo-electrons and "after pulses" in the photo-multiplier). Two successive gate circuits alternatively address the measurements belonging to delays t_1 and t_2 to counters I and II, respectively. Counters I and II act as accumulators and record the sums of pulse A amplitudes. Actually the ratio of their indications is equal to ratio $\bar{A}_1/\bar{A}_2$ of centroids $\bar{A}_1$ and $\bar{A}_2$ of the two A pulse spectra corresponding to delays t_1 and t_2, respectively. Namely

$$\bar{A}_1 = \sum_{s=1}^{N_1} N_{s1} A_{s1} / N_1 , \tag{14}$$

$$\bar{A}_2 = \sum_{s=1}^{N_2} N_{s2} A_{s2} / N_2 , \tag{15}$$

where N_{s1} and N_{s2} are the numbers of A pulses of amplitude A_{s1} and A_{s2}, respectively. Since the total A-pulse numbers N_1 and N_2 are equal (the two delays being alternatively switched), the ratio between the indications of the two counters is equal to the ratio $\bar{n}_1/\bar{n}_2$ of the two spectra centroids $\bar{n}_1$ and $\bar{n}_2$ of the electrons remaining in the measuring chamber after delays t_1 and t_2, respectively.

(3) DESIGN OF WORKING CONDITIONS

(3.1) Limiting Values of p_0 Versus E/p_0

The values of the thermalization times obtained in Appendix B have been used to obtain curve a of Fig. 6, which gives the lower boundary for pressure p_0 versus E/p_0 at which satisfactory measurements of D can be made with the described chamber. This boundary is obtained by equalizing a given relaxation time to one time constant of the diffusion fundamental mode relevant to the same E/p_0 value.

An upper boundary for p_0 versus E/p_0 is obtained by putting $\tau = \infty$ in Eq. (13), i.e., by equalizing the time constant $N\Lambda_{11}^2/D_{1N}$ of diffusion fundamental mode to the source term $1/(\alpha_1 NW)$ due to Townsend's multiplication. Curve b of Fig. 6 has been obtained in this way, taking, *"a posteriori,"* the experimental values of D_1 and $\alpha_{1N}W$ obtained by the method described in this paper [see Tables II and III of Sec. 4(4.3) and Figs. 9 and 10].

Two other boundaries for p_0 versus E/p_0 arise from the requirement that the cw radio-frequency field be equivalent, with respect to diffusion, to a constant (dc) electric field. This requirement leads to two conditions. One of them can be achieved by considering the particular case of a mean-free-path λ-independent of thermal velocity c. In this case for E = constant the electron distribution function is a Druyvesteyn one[8] and for a sinusoidal field $E = E_0 \sin\omega t$ is a Margenau one.[9] These two distribution functions are equal provided that

$$E^2 = E_0^2(1 + 2\omega^2/\nu^2) , \tag{16}$$

where $\nu = c/\lambda$. Since Eq. (16) must be verified for all possible values of collision frequency ν, it practically implies that the second term inside the brackets of Eq. (16) be small with respect to unity. In this case the oscillating field is equivalent to a constant field E of amplitude equal to the effective value $E_0/2^{1/2}$ of the sinusoidal field. If this condition is always assumed and errors less than 1% are required, then

$$\omega^2/\nu^2 \leq 10^{-2} \tag{17}$$

which implies that more than 50 collisions occur in a period of the alternating field. Curve c of Fig. 6 has been obtained by this condition as well as by the measured value of pulsation $\omega = 2\pi\, 16.26$ MHz and by ν values versus E/p_0. Rough ν values have been deduced from the expression[10] of drift velocity W in the case of a Maxwellian distribution and $d\lambda/dc = 0$

$$W = 0.85\,(e/m)\;\lambda/c\; = 0.85\, e/m\nu\,. \tag{18}$$

Drift-velocity values have been taken from Townsend-Bailey[11] and Phelps-Pack-Frost[12] [see Sec. 4 (4.2).

The other condition due to the requirement of equivalence between oscillating and constant fields, is that the ripple of electron energy ϵ be small compared with ϵ. Taking into account that errors occur only if the dependence of $D_1 p$ versus ϵ is nonlinear, it is sufficient that the energy ripple is 5–10% of ϵ. This condition implies a relationship between cw radio-frequency field period and thermalization time. For small ripples, it is possible to consider a relaxation time constant $(f\nu p_0)^{-1}$ which can be calculated by Eq. (B.3) of Appendix B. Therefore, taking into account that, when condition (17) is satisfied, the sinusoidal field is equivalent to a rectified full-wave field (in order to heat electrons), it is sufficient that the thermalization time constant be not smaller than a half period π/ω of the alternating field

$$1/f\nu_1 p_0 \geq \pi/\omega \tag{19}$$

in order to have an energy ripple[13] of 7.5%. The upper boundary for p_0 versus E/p_0 resulting from Eq. (19) is represented in Fig. 6 by curve d.

Notice that Eqs. (17) and (19) imply

$$f\nu_1 p_0 \leq \omega/\pi \leq 0.1\nu_1 p_0/\pi \tag{20}$$

and therefore an upper boundary for fractional loss f of kinetic energy

$$f \leq 0.1\pi \tag{21}$$

which corresponds to $E/p_0 \simeq 17$ V cm^{-1} Torr^{-1}. This upper boundary for E/p_0 is independent of pulsation ω chosen for the continuous sinusoidal field and therefore other c and d curves, relevant to a different pulsation, cross on the vertical line e of Fig. 6.

Another boundary for E/p_0 comes from the assumption made in Eqs. (5) and (6) of Sec. 2 (2.1) on the effective height of the measuring chamber. It is convenient, for the accuracy of measurements, that $2s$ [where s is given by Eq. (6)] be smaller than $H/4$ (where H is the chamber geometrical height). Fortunately this condition implies an upper boundary for $E/p_0 \simeq 23$ V cm^{-1} Torr^{-1} larger than the one given by Eq. (21).

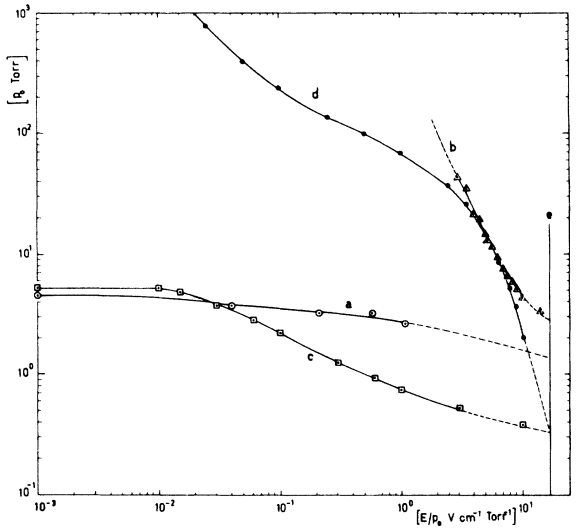

FIG. 6. Boundaries for p_0 versus E/p_0. Curve a is a lower boundary to allow electron energy relaxation in one time constant of diffusion fundamental mode. Curve b is an upper boundary due to balancing of electron diffusion losses by Townsend's multiplication. Curves a and b depend on the chamber dimensions only. Curves c is a lower boundary to have equivalence, with respect to electron energy, between a constant (dc) electric field E and a sinusoidal field of frequency 16.26 MHz and effective value $E_0/2^{1/2}$ equal to the dc strength E. Curve d is an upper boundary to have an energy ripple small compared with electron mean energy. Curves c and d depend only on the frequency $\omega/2\pi$ of the cw radio-frequency field and always cross each other on the vertical line e (the crossing point depends on $\omega/2\pi$).

(3.2) Choice of Working Conditions

Curves a and b of Fig. 6 depend on the chamber geometry, whereas curves c and d depend only on the frequency of the cw radio-frequency field. The geometrical height H of the measuring chamber must be much larger than $2s$ given by Eq. (6), but smaller than radius R, if diffusion is to be mainly conditioned by the electrodes rather than by lateral wall, where the small tube D slightly perturbs the geometry. If the chamber dimensions are increased, limiting curves a (due to relaxation) and b (due to Townsend's multiplication) fall in the same way, thus defining a useful region of the same size. Therefore it is sufficient (construction difficulties increase with the chamber dimensions) to select a height H sufficiently larger

than the maximum distance $2s$. A height $H = 2.952$ cm has been taken and consequently a radius $R = 3.735$ cm $> H$. Once the chamber dimensions have been selected, the frequency $(\omega/2\pi)$ of the continuous sinusoidal field is determined by the best overlapping of curves a and b with curves c and d (which displace vertically in the same way since, for both c and d curves, p_0 is proportional to frequency at a given E/p_0 value). The frequency assumed is $\omega/2\pi = 16.26$ MHz.

To find D_{1N} and $\alpha_{1N}W$, measurements are required at two different pressures [see Eq. (13)]. In order to have redundances, measurements have been performed at three different pressures. The three pressures have been selected with the following criterion. To exploit the maximum E/p_0 range, it appears from Fig. 6 that it is convenient to work at pressures near the lower boundaries. The value of one of the three working pressures was 7.22 Torr. In this case (even at the lowest E/p_0 values used) an error less than 0.5% in the equivalent constant field E is estimated in assuming that it is equal to the effective value $E_0/2^{1/2}$ of the sinusoidal heating field. Notice that at low E/p_0 values the slope of the curve D_{1p} versus (E/p_0) is low (see Fig. 7) and therefore an error less than 0.5% in the E/p_0 value implies an error less than 0.1% in D_{1p}. For $E/p_0 > 2.5\%$ V cm^{-1} Torr^{-1} the slope is larger but in this range the error (due to the assumption $E = E_0/2^{1/2}$) is negligible. For a second set of measurements a pressure of 3.61 Torr has been used, which allows to perform measurements at larger E/p_0 values. With this pressure, measurements are affected by errors less than 1% in E/p_0 for $E/p_0 > 3.3\times10^{-2}$ V cm^{-1} Torr^{-1}. Thermalization of primary electrons turned out to require 1.6 time constants of diffusion fundamental mode for $E/p_0 = 0$ and 1 time constant for $E/p_0 > 8$ V cm^{-1} Torr^{-1}. The third working pressure was 4.56 Torr, in order to have a convenient intermediate ramification between the curves of $D_{1p} - \alpha_{1p}p_0^2\Lambda_{11}^2W$ relevant to the first and second pressures [see Sec. 4 (4.2) and Fig. 7].

At this pressure, errors in E/p_0 values are less than 1% for $E/p_0 > 2\times10^{-2}$ V cm^{-1} Torr^{-1}.

(4) EXPERIMENTAL RESULTS AND THEIR INTERPRETATION

(4.1) Preliminary Operations

The first operation consists in balancing work-function differences, as described in Sec. 2 (2.2) (see also Fig. 4) by operating between one and two (presumed) time constants τ_{11} of diffusion fundamental mode.

As a second operation the x-ray pulse duration is fixed to a value lower (or equal) to one diffusion time constant τ_{11} and x-ray intensity I is varied. For low values, τ_{11} is independent of I, whereas, for high I values, τ_{11} increases with I because of ambipolar effects due to ion space charge. Then I is fixed at a maximum value (in order to have a good statistics) lower than the value in correspondence of which τ_{11} appreciably increases.

As a third operation the amplitude of the sampling pulse S is varied. The diffusion time constant τ_{11} is independent of S up to a value, starting from which τ_{11} apparently increases with S because of loading effects. Namely the electronic circuit is more loaded in correspondence with the sampling pulse relevant to delay t_1 than for the one relevant to delay $t_2 > t_1$ since the electron number remaining after t_1 is larger than the one after t_2. The amplitude of the sampling pulse is then fixed at a value sufficiently lower than the one at which τ_{11} starts to increase. It is also verified, by switching off x rays, that no spurious light pulses due to discharge occur, even when the sampling amplitude is increased to values much higher than the working values.

A fourth preliminary operation consists in checking that the diffusion time constant is independent of the clearing voltage amplitude and the duty cycle period (the time interval between two successive x-ray pulses can be varied from a minimum value of 20 msec = (50 Hz)$^{-1}$ up to 2.56 sec). It has also been checked, as expected, that it is possible to have zero amplitude for the clearing voltage by using a time interval (between two successive x-ray pulses) larger than about five diffusion time constants τ_{ion} of positive ions. For example, with $p_0 = 7.22$ Torr (maximum pressure used) one obtains $\tau_{\text{ion}} = p_0\Lambda_{11}^2/D_{1\text{ ion}} \simeq 0.12$ sec, the reduced ion diffusion coefficient $D_{1\text{ ion}}$ being deduced by the Nerst-Compton-Einstein relationship $D_{1\text{ ion}} = \mu_{1\text{ ion}}KT/e$, where $\mu_{1\text{ ion}}$ is the reduced value of mobility[14] at low E/p_0 ($\mu_{1\text{ ion}} \simeq 8.2\times10^3$ cm^{2}sec^{-1} V^{-1}Torr and consequently $D_{1\text{ ion}} \simeq 210$ cm^{2}sec^{-1}Torr).

(4.2) Experimental Results

After the best working conditions were determined by the preliminary procedure described in Sec. 4 (4.1), complete curves $\bar{n} = \bar{n}(t)$ at $E = 0$ and different pressures were performed (for $p_0 = 7.22$ Torr see Fig. 2). By data fitting, the parameters appearing in Eq. (11) have been determined. For practical purposes the combined effects, due to the two helium metastables, are equivalent to a single asymptotic time constant which is of about 1000 μsec in the case of 7.22-Torr pressure (reduced to 0°C) as shown in Fig. 2. Notice that the slope of the curve $\bar{n} = \bar{n}(t)$ of Fig. 2 is practically unaffected, between 25 and 50 μsec, by metastable effects and is due to diffusion only. For $E = 0$ one has $\alpha_1 = 0$ and therefore from Eq. (13) and the experimental values $\tau_{11} = 25.91$ μsec for $p_0 = 7.22$ Torr (see Fig. 2), $\tau_{11} = 16.45$ μsec

for $p_0 = 4.6$ Torr and $\tau_{11} = 12.9$ μsec for $p_0 = 3.61$ Torr, we obtain

$$D_{1N} = N\Lambda_{11}^2/\tau_{11} = 6.4 \times 10^{21}(1 \pm 0.05)\ \text{cm}^{-1}\,\text{sec}^{-1},$$
$$D_{1p} = p_0\Lambda_{11}^2/\tau_{11} = 1.809 \times 10(1 \pm 0.05)\ \text{cm}^2\,\text{Torr}\,\text{sec}^{-1}.$$

Notice the close agreement between the values of τ_{11}/p_0 relevant to different pressures. The data for $p_0 = 3.61$ Torr have been taken after two time constants of diffusion fundamental mode to allow complete thermalization [see Sec. 3 (3.1) and (3.2)].

The other measurements of $\bar{n}_1/\bar{n}_2$ in the range of one and two time constants of diffusion fundamental mode have been performed by switching on the oscillator in order to "heat" electrons. Curves similar to that of Fig. 2 have been performed for the maximum and intermediate E/p_0 values, so as to ascertain that metastable effects are negligible between one and two time constants of the first term at the right-hand side of Eq. (11). For $E/p_0 > 3$ V cm^{-1} Torr^{-1}, Townsend's multiplication turned out to be appreciable and therefore an apparent reduced diffusion coefficient D_{1N} defined by [see Eq. (13)]

$$D_{1N}^* = N\Lambda_{11}^2/\tau = D_{1N}N^2\Lambda_{11}^2 W \qquad (23)$$

has been measured. Actually the experimental result for the apparent diffusion coefficient reduced to $p_0 = 1$ Torr

$$D_{1p}^{**} = D_{1N}^* p_0/N = \Lambda_{11}^2 p_0/\tau$$
$$= D_{1p} - \alpha_{1p} p_0^2 \Lambda_{11}^2 W \qquad (24)$$

are collected in Table I and shown in Fig. 7. For $E/p_0 < 3$ V cm^{-1} Torr^{-1} there is a very good agreement between the experimental D_{1p}^* values relevant to different pressures. Notice that D_{1p} values relevant to $p_0 = 4.56$ Torr begin from $E/p \geq 2.6 \times 10^{-2}$ V cm^{-1} Torr^{-1}, where the error due to closeness to curve c [see Sec. 3 (3.1)] is less than 0.72% (the error quickly decreases with E/p_0 increasing: see Fig. 6). Values relevant to $p_0 = 3.61$ Torr begin from $E/p_0 = 0.23$ V cm^{-1} Torr^{-1} where the error in E/p_0 is less than 0.3%. The thermal value is indicated in Fig. 7 as an asymptotic, dashed, horizontal line. The experimental data branch out for $E/p_0 > 3$ V cm^{-1} Torr^{-1}, when the reduced Townsend first coefficient α_{1p} increases so that the second term at the right-hand side of Eq. (24) is no longer negligible with respect to the first term.

The errors are within ± 0.5% in E values [as examined in Sec. 2 (2.2)] within ± 0.3% in pressure values[15] and therefore within ± 0.61% in E/p_0 values.

The errors in D_{1p} values for $E/p_0 < 3$ V cm^{-1} Torr^{-1} are within ± 1% and are mainly due to statistical fluctuations, since the chamber dimensions are known within 0.1% and pressure values[15] within 0.3%.

For $E/p_0 > 3$ V cm^{-1} Torr^{-1} the accuracy is worse since statistical fluctuations increase. For $E/p_0 > 8.21$ cm^{-1} Torr^{-1} and $p_0 = 4.56$ Torr (intermediate pressure used) curve d of Fig. 6 is crossed and the energy ripples due to the sinusoidal heating field are no longer negligible. Fortunately an energy ripple implies errors only if the dependence of D_{1p} on ϵ is nonlinear within the energy ripple. Another error comes from the inaccuracy in the distance $2s$ defined by Eq. (6) of Sec. 2 (2.1), since there are no accurate data of drift velocity W in this E/p_0 range. The very accurate data of Crompton, Elford, and Jory[16] stop at $E/p_0 = 1.072$ V cm^{-1} Torr^{-1}. However, it is possible to estimate that errors in W values are less than ± 10%, if we take those of Townsend and Bailey[11] and Phelps, Pack, and Frost[12] (see also data of Heylen and Lewis,[17] Nielsen,[18] Bowe,[19] Hornbeck,[20] and Stern[21]). The fractional variation of the square of the fundamental diffusion length Λ_{11}^2 [which appears in Eqs. (5), (8), (10), (12), (13)], is 0.22 starting from the value 0.654 cm^2 for $E = 0$ up to 0.532 cm^2 for $E/p_0 = 9.4$ V cm^{-1} Torr^{-1} and therefore the error in Λ_{11}^2 is contained within ± 2.2%.

Thus it is possible to estimate that the accuracy in the apparent diffusion coefficient D_{1p}^* varies from ± 1% for $E/p_0 \simeq 3$ V cm^{-1} Torr^{-1} to ± 3% for $E/p_0 \simeq 9.4$ V cm^{-1} Torr^{-1}.

Figure 7 reports also D_{1p} values indirectly de-

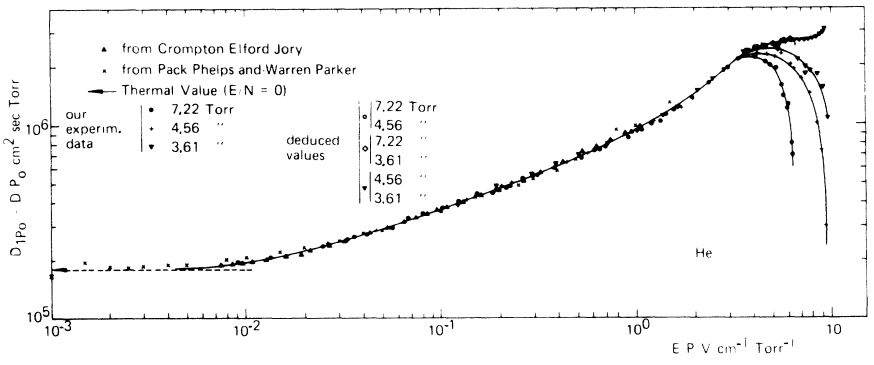

FIG. 7. Experimental values of reduced, apparent diffusion coefficients: $D_{1p}^{**} = D_p^* p = D_{1p} - \alpha_{1p} \times W p_0^2 \Lambda_{11}^2$ versus E/p_0 and comparison with other values, indirectly deduced from μ_{1p} and (D/μ) data of other authors.

duced from μ_{1p} and (D/μ) data of Crompton, Elford, and Jory,[16] which are in surprising agreement and D_{1p} values deduced from μ_{1p} data of Pack and Phelps[22] and (D/μ) data of Warren and Parker,[23] which differ up to 10% from our data. Since Warren and Parker's D/μ data are in good agreement with those of Crompton, Elford, and Jory,[16] it is possible to draw the conclusion that the accuracy of Pack and Phelp's[22] μ data is within ± 5%.

(4.3) Interpretation and Discussion of Experimental Results

For $E/N \leq 8\times10^{-17}$ V cm^2 ($E/p_0 \leq 2.83$ cm^{-1} Torr^{-1}) the apparent, reduced diffusion coefficients D_{1N}* [given by Eq. (23)] and D_{1p}* [given by Eq. (24)] are practically equal to the actual diffusion coefficients D_{1N} and D_{1p}, respectively.

For $E/N > 8\times10^{-17}$ V cm^2, the quantities D_{1N}, D_{1p}, $\alpha_{1N}W$, and $\alpha_{1p}W$ have been deduced from Eqs. (23) and (24). The experimental data at three different pressures introduce redundances allowing greater accuracy. The values of reduced diffusion coefficient D_{1p}, calculated by the experimental data relevant to the different couples of pressure, are given in Fig. 7. Figure 8 reports D_{1N} data (without indications relevant to different pressures).

For $E/N > 3\times10^{-17}$ V cm^2 ($E/p_0 > 1.1$ V cm^{-1} Torr^{-1}) no accurate diffusion data are available for comparison.

Figure 8 reports the old values deduced from Townsend and Bailey's[11] data for μ_{1N} and (D/μ).

The curves of Figs. 7 and 8 and the D_{1N} and D_{1p} data quoted in Table II have been completed by interpolation at low E/p_0 values up to our experimental thermal value ($E/N = 0$).

Interpolation is facilitated by the knowledge that, for $E/N \leq 5.65\times10^{-20}$ V cm^2 ($E/p \leq 2\times10^{-3}$ V cm^{-1} Torr^{-1}), values of Warren and Parker,[23] in agreement with those of Crompton, Elford, and Jory,[16] are practically equal to their thermal values: The same thing has been assumed for D_{1N} and D_{1p} values.

The data quoted in Table II have been read on a curve which accurately interpolates all experimental values, and errors can be considered as halved with respect to crude experimental values. Therefore an over-all accuracy of ± 0.5% can be claimed in the range $0 \leq E/N \leq 9\times10^{-17}$ Vcm^2 and one varying from ± 0.5% up to ± 1.5% in the range $9\times10^{-17} \leq E/N \leq 2.7\times10^{-17}$ V cm^2.

Notice that the agreement between our experimental data and the ones obtained by $\mu_{1N}(D/\mu)$ data of Crompton, Elford, and Jory[16] is within 0.5% from the lowest E/N values up to $E/N = 1.2\times^{-17}$ V cm^{-2} and within 2% (i.e., within ± 1% with respect to intermediate values) from $E/N \geq 1.2\times10^{-17}$ V cm^{-2} up to the maximum value of Crompton, Elford, and Jory ($E/N = 3.03\times10^{-17}$ V cm^{-2}).

As stated by these authors, their best values are in the range $0.0064 \leq E/p_0 \leq 0.645$ V cm^{-1}, and for $E/p_0 > 0.645$ V cm^{-1} Torr^{-1} ($E/N > 1.82\times10^{-18}$ V cm^{-2}) their errors both in W and D/μ data are of 1% order. Consequently there is agreement to within the claimed errors.

Values of $\alpha_{1N}W$ have been deduced by Eq. (23) in the range $9.03\times10^{-17} \leq E/N \leq 2.7\times10^{-16}$ V cm^{-2} ($3.2 \leq E/p_0 < 9.4$ V cm^{-1} Torr^{-1}) and are plotted versus E/N in Fig. 9. The accuracy in deducing $\alpha_{1N}W$ is not good (±8%) for the lowest E/N values of Fig. 9 [where the second term at the right-hand side of Eq. (23) is of the order of a few percent with respect to the first one] and for the highest E/N values (where the slope of D_{1N}* versus E/N is high and therefore inaccuracies of E/N are critical). In the range $1.13\times10^{-16} \leq E/N \leq 3.19\times10^{-16}$ V cm^{-2} ($4 \leq E/p_0 \leq 9$ V cm^{-1} Torr^{-1}: see Fig. 7) the error, due to the deduction from the experimental, apparent diffusion coefficient D_{1N}* and the other causes of error considered in Sec.

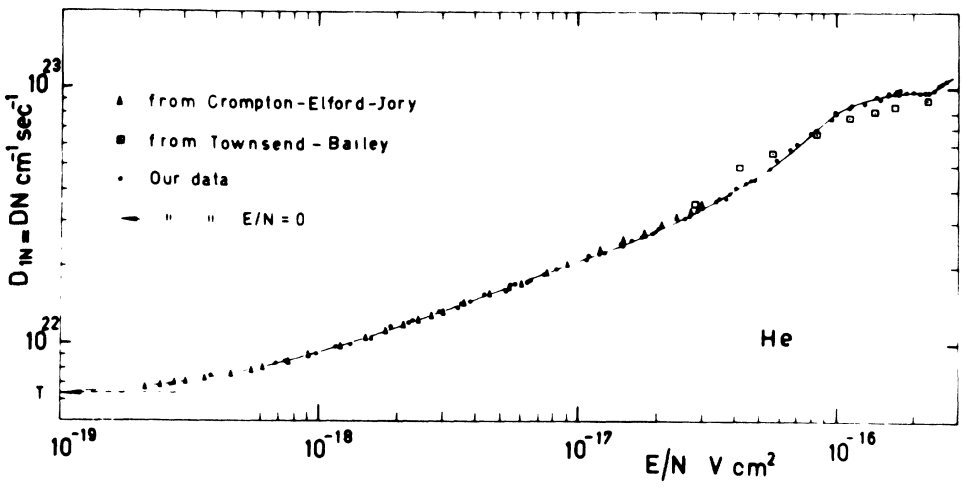

FIG. 8. Electron reduced diffusion coefficients $D_{1N} = DN$ versus E/N. Notice the good agreement with the values obtained from μ_{1N} and (D/μ) data of Crompton, Elford and Jory.[16]

TABLE I. Experimental values of the apparent diffusion coefficient $D_{1p}^* = D_{1p} - \alpha_{1p} W p_0^2 \Lambda_{11}^2$ reduced to $p_0 = 1$ Torr for given E/p_0 values.

$p_0 = 7.22$ Torr		$p_0 = 4.56$ Torr		$p_0 = 3.61$ Torr	
E/p_0	D_{1p}^*	E/p_0	D_{1p}^*	E/p_0	D_{1p}^*
0	1.809×10^5	0	1.808×10^5	0	1.807×10^5
9.08×10^{-3}	1.979	2.62×10^{-2}	2.445	1.224×10^{-1}	3.89
1.345×10^{-2}	2.1	4.62	2.86	1.945	4.855
2.41	2.38	7.87	3.43	2.922	5.57
3.235	2.575	1.355×10^{-1}	4.13	3.92	6.26
3.505	2.608	2.03	4.85	4.285	6.36
4.14	2.78	2.315	5.02	5.2	7.04
5.64	2.96	2.965	5.54	7.31	8.07
6.67	3.33	4.465	6.43	1.035×10^0	9.48
7.84	3.45	5.74	7.21	1.39	1.104×10^6
8.12	3.53	6.96	7.79	1.685	1.236
1.039×10^{-1}	3.77	9.54	9.04	2.09	1.516
1.25	4.06	1.249×10^0	1.055×10^6	2.495	1.715
1.546	4.41	1.715	1.238	2.88	1.92
1.866	4.55	2.9	1.93	3.8	2.35
2.178	4.83	3.68	2.3	4.77	2.27
2.269	4.93	4.24	2.34	4.79	2.27
2.645	5.34	4.75	2.29	5.42	2.4
3.167	5.6	5.2	2.2	6.14	2.18
3.822	6.02	5.64	2.31	6.82	2.165
5.22	6.84	6.28	2.03	7.42	1.83
6.285	7.47	6.54	1.95	7.54	1.95
6.48	7.51	7.16	1.73	7.92	1.88
7.04	7.87	7.82	1.445	8.48	1.8
1.079×10^0	9.63	8.87	7.58×10^5	9.12	1.545
1.217	1.026×10^6	9.41	3.02	9.6	1.08
1.346	1.055				
1.448	1.169				
1.595	1.215				
1.975	1.385				
2.399	1.65				
2.92	1.95				
3.43	2.17				
4.1	2.219				
4.7	2.115				
4.98	2.05				
5.17	1.999				
5.35	1.6				
5.72	1.41				
6	1.186				
6.085	1.212				
6.22	8.05×10^5				
6.3	7.05				

p_0 = pressure in Torr (= 1 mm Hg) reduced to 0° C

$[E/p_0] = [V\,\mathrm{cm}^{-1}\,\mathrm{Torr}^{-1}]$

$D_1^* = D_1 - \alpha_1 p_0^2 \Lambda_{11} W$

4 (4.2) is within ± 4%. But here another cause of error is due to impurity since first Townsend's coefficient is very sensible to them and it is very difficult to make some prevision, despite the fact that the measuring chamber has been baked at $T = 350°$ C for about 50 h and Linde's helium of spectral purity has been used. However, by means of the experimental data reported in Fig. 2, it is possible to roughly estimate that the impurity concentration N^* is of the order of 10^{-6} of the helium concentration N (see Appendix A) and hence $\alpha_{1N} W$ values should not be affected by impurity effects.

Dividing $\alpha_{1N} W$ data by the drift velocity data of Townsend and Bailey[11] and of Phelps, Pack, and Frost,[12] α_{1N} data have been obtained and are reported in Fig. 10. Notice that our data are intermediate between the ones of other authors, which

TABLE II. Experimental values of electron diffusion coefficients in helium, reduced to 1 Torr at $T = 273°$ K ($D_{1p} = Dp_0$) or to one gas molecule per unit volume ($D_{1N} = DN$).

E/p_0 (V cm^{-1} Torr^{-1})	$D_{1p_0} = Dp_0$ (cm^2 sec^{-1} Torr)	E/N (V cm^2)	$D_{1N} = DN$ (cm^{-1} sec^{-1})
0	1.809×10^5	0	6.41×10^{21}
1.7×10^{-3}	1.809	6×10^{-20}	6.42
2	1.81	8	6.44
2.5	1.815	1×10^{-19}	6.46
3	1.82	1.5	6.58
4	1.835	2	6.69
5	1.85	2.5	6.81
6	1.86	3	7.03
8	1.91	4	7.4
1×10^{-2}	1.98	5	7.78
1.5	2.1	6	8.09
2	2.25	8	8.65
2.5	2.37	1×10^{-18}	9.22
3	2.49	1.5	1.04×10^{22}
4	2.7	2	1.15
5	2.9	2.5	1.25
6	3.1	3	1.33
8	3.45	4	1.49
1×10^{-1}	3.7	5	1.62
1.5	4.3	6	1.73
2	4.8	8	1.93
2.5	5.2	1×10^{-17}	2.09
3	5.57	1.5	2.44
4	6.2	2	2.77
5	6.9	2.5	3.08
6	7.4	3	3.37
8	8.4	4	3.95
1×10^{0}	9.38	5	4.55
1.5	1.17×10^6	6	5.21
2	1.44	8	6.67
2.5	1.7	1×10^{-16}	8.01
3	2	1.2	8.79
4	2.4	1.4	9.18
5	2.57	1.6	9.41
6	2.7	2	9.61
8	2.74	2.3	9.66
9	2.9	2.4	9.79
9.6	3.4	2.6	1.05×10^{23}
		2.8	1.10

are dispersed by a factor of 6 if theoretical data are included and by a factor of 3 if only experimental values are considered.

Theoretical data (Dunlop,[24] Heylen and Lewis[17]) are affected by the difficulty of calculating a reliable electron distribution function when the inelastic collision frequency is no longer negligible with respect to elastic collision frequency. Different calculation procedures lead to different distribution functions, particularly in correspondence with the high-energy tail, which is responsible for ionization (for example, compare the distribution functions obtained by Heylen and Lewis[17] with those obtained by Airoldi Crescentini and Maroli[25]). Moreover electron velocity variations between two successive collisions can no longer be considered as negligible with respect to thermal velocities.[26]

The experimental data of Davies, Llewellyn Jones and Morgan[27] and of Chanin and Rork[28] are questionable because, as correctly observed by Dutton, Llewellyn Jones, and Rees,[29] measurements were carried out over such a restricted range of values of pd, at low values of E/p, that the values of Townsend coefficients are subject to great uncertainty. On the other hand, the experimental values of Dutton, Llewellyn Jones, and Rees[29] are affected by impurity effects since the

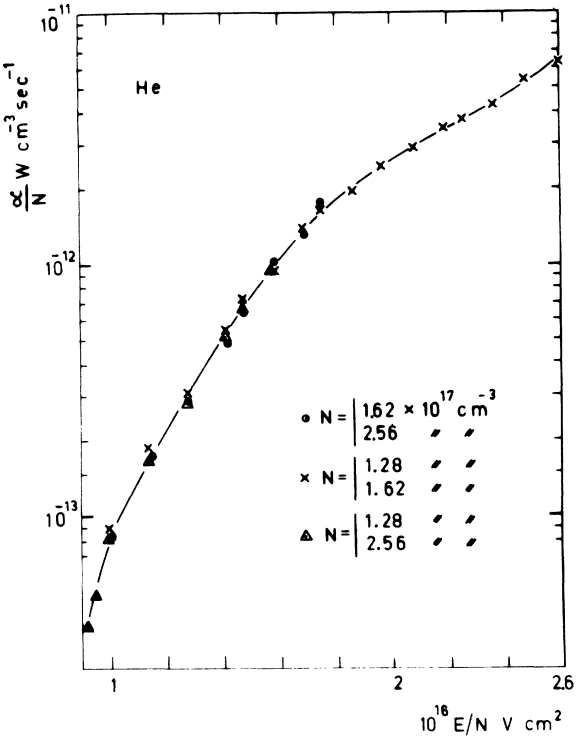

FIG. 9. Values of $\alpha_{1N}W$ versus E/N, deduced, by Eq. (23), from our experimental values of apparent diffusion coefficients at various pressures.

1.5% neon contained in the gas used by these authors cannot be eliminated by a gas circulating system. The presence of neon increases the values of α_{1p} because the ionization potential of neon is lower than that of helium.

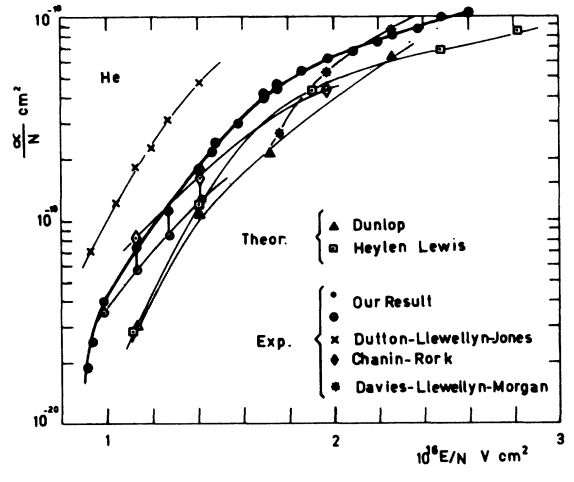

FIG. 10. Reduced first Townsend's coefficient $\alpha_{1N} = \alpha/N$ versus E/N and comparison with the data of other authors. ● values obtained from our $\alpha_{1N}W$ data (see Fig. 9) and drift velocity data of Townsend and Bailey[11] and of Phelps, Pack and Frost.[12] ○ values obtained from our $\alpha_{1N}W$ data and W data of Nielsen.[18]

In conclusion, it is possible to claim an improvement of more than one order of magnitude in the present data of α_{1p} (with respect to data of other authors), since the error in our data may be within ±10%, due perhaps mainly to errors in W data. The experimental values of $\alpha_{1N}W$, $\alpha_{1p}W$, α_{1N}, and α_{1p} are quoted in Table III versus E/N and E/p_0, respectively. Similarly, the present D_{1N} (and D_{1p}) data (see Table II and Fig. 8) can be claimed to be by one order-of-magnitude more accurate than other (indirect) data for $E=0$ and $E/N > 3.03\times10^{-17}$ V cm^2. For $2.6\times10^{-19} \leq E/N \leq 3.03\times10^{-17}$ V cm^2 they are a strong confirmation in favor of Crompton, Elford, and Jory's[16] data.

Note added in proof: Notice that by the present method, when the high-frequency "heating" field is acting, what is actually measured is a lateral diffusion coefficient and therefore there is agreement with the very precise data of Crompton, Elford, and Jory[16] who use a Townsend-Huxley method. There is no agreement with the data of Wagner, David, and Hurst,[30] who use a time-of-flight method and therefore measure a longitudinal diffusion coefficient [see a paper of H. R. Skullerud, to be published in J. Phys. B].

ACKNOWLEDGMENTS

The author is strongly indebted to Professor E. Gatti for valuable assistance and helpful discussions during the development of this work. The author also wishes to express his thanks to Mr. V. Donati for the construction of the measuring chamber, Dr. A. Ferrario and E. Marelli for the development of the electronic apparatus and Dr. A. Oggioni, Dr. D. De Giovannini, Dr. A. Ferrario, and Dr. E. Cervi for aid in experimental measurements.

APPENDIX A

Evaluation of Impurity Concentration

Since the parameters D_{1ms}, γ_s, δ_s, and β_s appearing in Eq. (10) are roughly known from the literature, it is possible to deduce the impurity number density N^* from the experimental knowledge of the metastable time constants τ_{ms} in our working conditions. However, the time constant of 1000 μsec indicated in Fig. 2 is due to both types of helium metastable atoms.

Moreover our measurements, when $\bar{n}$ is of the order of 10^{-3} with respect to the initial value $\bar{n}_0$, are affected by statistical fluctuations of the order of 20% (compared with 1% in the range $25 < t < 50$ μsec of Fig. 2). Experiments to perform mea-

surements of metastable time constants must be performed by gas mixtures with partial concentrations of the same order, so that the coefficients A and B, appearing in Eq. (22), are of the same order.

The experimental curve of Fig. 2 is better used by measuring the coefficients A and B_S of Eq. (11). As already mentioned in Sec. 4 (4.2), the combined effects, due to the two helium metastables, are equivalent, for practical purposes, to a single asymptotic time constant. Therefore the two theoretical coefficients B_S of Eq. (11) reduce to only one coefficient B. By solving Eq. (8) and taking into account Eq. (10), it gives

$$A = n_0 - B \simeq n_0, \tag{A.1}$$

where n_0 is the initial electron number and

$$B = \beta N^* n_m / (1/\tau - 1/\tau_m) , \tag{A.2}$$

where β is deexcitation rate by Penning's effect considered in Eq. (2), N^* impurity concentration, n_m initial number of metastable atoms τ electron-diffusion time constant [given practically by the first term at the right-hand side of Eq. (12)], and τ_m metastable time constant [appearing in Eqs. (10) and (11)]. Assuming that $n_m \simeq n_0 = A$ and taking into account that $\tau_m \gg \tau$, one gets

$$\beta N^* \simeq B/A\tau . \tag{A.3}$$

The initial ordinate of value 5.07 of Fig. 2 is proportional to A and the intersection at 6.14×10^{-3} of the $\bar{n}$ axis with the almost asymptotic behavior due to metastables (time constant $\simeq 1000$ μsec) is proportional to B. Therefore, since $\tau = 25.91$ μsec (see Fig. 2) we obtain

$$\beta N^* \simeq 46 \text{ sec}^{-1} . \tag{A.4}$$

The de-excitation rate β (at $N = N^* = 1$) is given by σv_γ where v_γ is the relative velocity between metastable helium atoms and impurity atoms and σ is the cross section for Penning's effect. Impurity due to outgassing from the walls is mainly water vapor, for which unfortunately there are no β (or σ) data. There are, however, no strong variations for the ionization cross section for Penning's effect between helium metastables and molecules like O_2, CO_2, C_2H_4 having dimensions and ionization potentials of the same order.[31] At $T \simeq 300$°K the relative velocity v_γ being about 1.5×10^5 cm/sec, taking $\sigma \simeq 13\times10^{-16}$ cm^2, we obtain $\beta \simeq 1.95\times10^{-10}$ cm^3 sec^{-1}. Hence from Eq. (A.4) we get $N^* \simeq 2.4\times10^{11}$ cm^{-3}, which is of the order of 10^{-6} with respect to helium number density $N \simeq 2.56\times10^{17}$ (corresponding to $p_0 = 7.22$ Torr).

APPENDIX B

Thermalization Times

Relaxation times required by fast electrons (produced by x rays) to reach practical equilibrium energy (within 2% of the final equilibrium value) have been calculated roughly. The results have been used to estimate the minimum delay (after the end of the x-ray pulse) after which measurements are not affected by energy relaxation. Calculations have been performed considering only the mean value, as in Compton's theory,[32] so that an energy balance gives

$$d\epsilon = -\nu f \epsilon dt + eEWdt , \tag{B.1}$$

where ϵ is the mean kinetic electron energy, $\nu = \bar{c}/\lambda$ is the collision frequency (λ is the mean free path), f is the fractional loss of kinetic energy per collision, e is the electron charge, E is the electric field strength, and W is the drift velocity.

Integration of Eq. (B.1) in a time interval $t_2 - t_1$, sufficiently small to allow taking, for ϵ, f and W, values relevant to the mean value $(\epsilon_1 + \epsilon_2)/2$ of the energy corresponding to $(t_2 - t_1)$, gives

$$t_2 - t_1 = \frac{1}{f\nu_1 p_0} \ln \frac{eWE/p_0 - f\nu_1\epsilon_2}{eWE/p_0 - f\nu_1\epsilon_1} . \tag{B.2}$$

Here p_0 is gas pressure reduced to 0°C, ν_1 is collision frequency at $p_0 = 1$ Torr, and $f\nu_1$ is deduced from Eq. (B.1) in equilibrium (eq) condition and assuming a Maxwellian distribution

$$f\nu_1 = \left(\frac{eEW}{p_0\epsilon}\right)_{eq} = \frac{2}{3}\left(\frac{WE/p_0}{D/\mu}\right)_{eq} . \tag{B.3}$$

Values for W and D/μ have been taken from Crompton, Elford, and Jory,[16] Townsend and Bailey,[11] Phelps, Pack, and Frost,[12] Stern,[21] and Warren and Parker.[23] Curves of ϵ versus t at $p_0 = 1$ Torr and at different E/p_0 values are plotted in Fig. 11, starting from $\epsilon \simeq 6.6$ eV corresponding, at equilibrium, to $E/p_0 = 10$ V cm^{-1} Torr^{-1}. By a rough evaluation (for $E/p > 10$ V cm^{-1} Torr^{-1}, there are no reliable values for W and particularly for D/μ) it turns out that the time required to reach 6.6 eV, starting from about 18 eV, which is the mean energy of the free electrons produced by 25 keV x rays,[33] is less than 1 μsec. The curves of Fig. 11 are stopped at energy values 2% higher than equilibrium values thus giving practical thermalization times at $p_0 = 1$ Torr.

It is worthwhile noticing that relaxation times can be obtained by the method presented in this paper, working at low pressure where relaxation times are longer than one time constant of diffusion fundamental mode. Obviously both τ_{11} and metastable behavior [see Sec. 2 (2.1)] must be known from previous measurements at higher pressures.

TABLE III. Experimental values of $\alpha_{1N}W$ (where $\alpha_{1N}=\alpha N$ is first Townsend coefficients reduced to one molecule per unit volume) and $\alpha_{1p}W$ (where $\alpha_{1p}=\alpha p$ is reduced to 1 Torr at 273° K).

E/N	$\alpha_{1N}W$	α_{1N}	E/p_0	$\alpha_{1p}W$	α_{1p}
9.03×10^{-17}	3.61×10^{-14}	1.85×10^{-20}	3.2×10^{0}	1.28×10^{3}	6.55×10^{-4}
9.45	4.94	2.47	3.35	1.75	8.75
9.87	8.55	4.07	3.5	3.03	1.441×10^{-3}
1.129×10^{-16}	1.73×10^{-13}	7.27	4	6.14	2.58
1.27	3.03	1.165×10^{-19}	4.5	1.033×10^{4}	4.00
1.41	5.19	1.79	5	1.84	6.35
1.468	6.77	2.18	5.2	2.405	8.01
1.58	9.85	2.92	5.6	3.49	1.075×10^{-2}
1.69	1.365×10^{-12}	3.90	6	4.83	1.383
1.75	1.65	4.75	6.2	5.55	1.54
1.86	1.975	5.41	6.6	7.00	1.92
1.975	2.44	6.12	7	8.65	2.17
2.085	2.9	6.75	7.4	1.03×10^{5}	2.395
2.2	3.47	7.53	7.8	1.23	2.67
2.26	3.72	8.2	8	1.32	2.81
2.37	4.23	8.45	8.4	1.5	3.00
2.48	5.18	9.75	8.8	1.835	3.46
2.599	6.3	1.05×10^{-18}	9.2	2.235	3.72

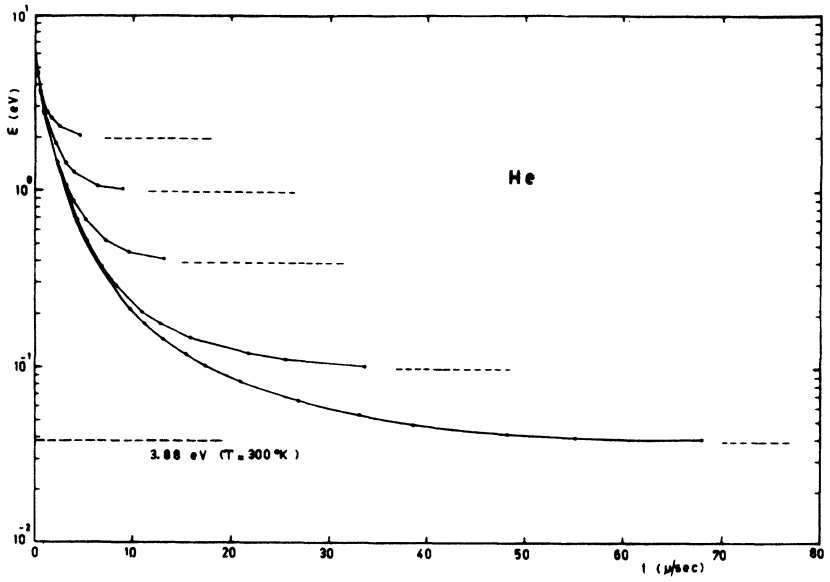

FIG. 11. Relaxation of electron energies starting from ≃ 6.6 eV (corresponding, in equilibrium conditions, to $E/p_0 \simeq 10$ $Vcm^{-1}Torr^{-1}$) and ending to a value by 2% higher than the equilibrium value, indicated by horizontal dashed lines. The five curves are, in increasing order, relevant to the following E/p_0 values: 0.4×10^{-2}, 0.21, 0.58, 1.08 Vcm^{-1} $Torr^{-1}$.

*Work partially supported by Contract No. 115.1402.01628 Consiglio Nazionale Della Richerche – Centro Informazioni Studi Esperienze, Milano, Italy.

[1]See, for example, L. G. Huxley and R. W. Crompton, in Atomic and Molecular Processes, edited by D. R. Bates (Academic Press, Inc., New York, 1962), Chap. 10, Sec. 9.1, p. 353; L. B. Loeb, Basic Processes of Gaseous Electronics (University of California Press, Berkeley, 1955), Chap. II, Sec. 4; E. W. McDaniel, Collision Phenomena in Ionized Gases (John Wiley & Sons, Inc., New York, 1964), Chap. 11.

[2]See, for example, L. B. Loeb in Ref. 1, Chap. VI, Sec. 5; E. W. McDaniel in Ref. 1, Sec. 10-10B; also original papers as M. A. Biondi, Phys. Rev. 90, 730 (1953); E. Holt, Bull. Am. Phys. Soc. 4, 112 (1959); M. C. Sexton, M. J. Mulcahy, and J. J. Lennon, in Proceedings of the Fourth International Conference on Ionization Phenomena in Gases (North-Holland Publishing Company, Amsterdam, 1959), Vol. 1, p. 94; Brit. J. Appl. Phys. 10, 356 (1959); J. J. Lennon and M. J. Mul-

cahy, Proc. Phys. Soc. (London) 78, 1543 (1961).

[3]J. A. Carruthers, Can. J. Phys. 40, 1528 (1962).

[4]G. Cavalleri, E. Gatti, and P. Principi, Nuovo Cimento 31, 302 (1964).

[5]See, for example, E. W. McDaniel in Ref. 1, Sec. 10.8, and L. B. Loeb in Ref. 1, Chap. VI, Sec. 5.

[6]See, for example, S. Glasstone, Principles of Nuclear Reactor Engineering (D. Van Nostrand Co., Princeton, New Jersey, 1955), 2nd ed., Sec. 3.24; R. L. Murray, Nuclear Reactor Physics (Prentice-Hall, Raleigh, N. C., 1957), 2nd ed., Chap. II, Sec. 2.3.

[7]W. B. Gill and A. Von Engel, Proc. Roy. Soc. (London) 192, 446 (1948).

[8]M. J. Druyvesteyn, Physica 10, 69 (1930); M. J. Druyvesteyn and Penning, Rev. Mod. Phys. 12, 87 (1940); see also Loeb in Ref. 1, Chap. IV, Sec. 3, p. 290.

[9]H. Margenau, Phys. Rev. 69, 508 (1946); see also E. W. McDaniel in Ref. 1, p. 554, Sec. 11-4-c.

[10]See, for example, Eq. (3.1) of L. B. Loeb in Ref. 1, Chap. III, Sec. 3, and relevant footnote 5. It is now possible to state that the correct factor is $\frac{2}{3}$ multiplied by the ratio between the average of $1/c$ over, as assumed, a Maxwellian distribution, and the mean velocity $\bar{c}$, which gives 1.275. The result is $1.275 \times \frac{2}{3} = 0.85$. For the factor $\frac{2}{3}$, see, for example, G. Cavalleri and G. Sesta, Phys. Rev. 170, 286 (1968).

[11]J. S. Townsend, A. V. Bailey, Phil. Mag. 44, 1013 (1922); and 46, 657 (1923).

[12]A. V. Phelps, J. L. Pack, and L. S. Frost, Phys. Rev. 117, 470 (1960).

[13]See, for example, J. Millman and C. C. Halkias, Electronic Devices and Circuits (McGraw-Hill Book Co., New York, 1967), Sec. 20-9, p. 612, Eqs. (20)–(49) where $2\omega L$ has been substituted by R (see Sec. 20-12 p. 620) and RC by π/ω.

[14]See, for example, E. W. McDaniel in Ref. 1, Sec. 9-9A, p. 466.

[15]Pressures have been measured by a bakeable, differential capacitance manometer (Granville Phillips with bakeable "sensing head" of 100 Torr full scale) used as a null instrument and a buthyle phtalate differential manometer. Since absolute errors are within ±0.3 mm of buthyle phtalate, the fractional error, for example with $p_0 = 7.22$ Torr = 92.2 mm of buthyle phtalate is within $\pm 3 \times 10^{-3}$.

[16]R. W. Crompton, M. T. Elford, and R. L. Jory, Aust. J. Phys. 20, 369 (1967).

[17]A. E. D. Heylen and T. J. Lewis, Proc. Roy. Soc. (London) Ser. 271, 531 (1962).

[18]R. A. Nielsen, Phys. Rev. 50, 950 (1936). Unfortunately these data were lost during the second world war (private communication) and data have been read directly on the curves reported in the quoted paper and in text books.

[19]J. C. Bowe, Phys. Rev. 117, 1411 (1960).

[20]J. Hornbeck, Phys. Rev. 83, 374 (1951).

[21]R. A. Stern, Sixiéme Conférence Internationale sur les Phénomènes d'Ionisation dans les Gaz, Paris, 8 au 13 juillet 1963, Tome I (C. I. P. I. G. Orsay; S. E. R. M. A., Editeur, Paris).

[22]J. L. Pack and A. V. Phelps, Phys. Rev. 121, 798 (1961).

[23]R. W. Warren and J. H. Parker, Phys. Rev. 128, 2661 (1962).

[24]S. H. Dunlop, Nature 164, 452 (1949).

[25]A. Airoldi Crescentini and C. Maroli, J. Plasma Phys. 2, 581 (1968).

[26]The same drawback affects theoretical calculations of drift velocity (see, for example, A. E. D. Heylen and T. J. Lewis data in Ref. 17 and reported in Fig. 8) for which it would be better to use the rigorous theory exposed in a recent paper: G. Cavalleri and G. Sesta, Phys. Rev. 170, 286 (1968). Moreover if the drift velocity of the center of the almost spherical electron avalanche is required, the term αW must be added to the drift velocity of the original primary electrons [see, for example, J. Brambing, Z. Physik 179, 532 (1964); and A. L. Ward, J. Appl. Phys. 361, 1291 (1965)].

[27]D. K. Davies, F. Llewellyn Jones, and C. G. Morgan, Proc. Phys. Soc. (London) 80, 898 (1962).

[28]L. M. Chanin and G. D. Rork, Phys. Rev. 133, 1005 (1964).

[29]J. Dutton, F. Llewellyn Jones, and D. B. Rees, Proc. Phys. Soc. (London) 85, 909 (1965).

[30]E. B. Wagner, F. J. Davis, and G. S. Hurst, J. Chem. Phys. 47, 3138 (1967).

[31]See, for example, K. L. Bell, A. Dalgarno, and A. E. Kingston, J. Phys. B. Atom. Mol. Phys. 1, 18 (1968); and E. E. Benton, E. E. Ferguson, and W. W. Robertson, Phys. Rev. 128, 206 (1962).

[32]J. M. Benade and K. T. Compton, Phys. Rev. 11, 184 (1910); K. T. Compton, *ibid.* 22, 333 (1923); K. T. Compton and I. Langmuir, Rev. Mod Phys. 2, 219 (1930). See also L. B. Loeb in Ref. 1, Chap. III, p. 219.

[33]The mean energy of free electrons produced by 25-keV x rays has been roughly evaluated by the procedure used in the Appendix of G. Cavalleri, E. Gatti, and P. Principi, Nuovo Cimento 31, 318 (1964). The value of D_{760} for neon given in that paper is not correct. A better value is given in G. Cavalleri, E. Gatti, and A. M. Interlenghi, Nuovo Cimento 40, 450 (1965), though use is made of a measuring chamber in which Volta effects cannot be balanced.